Plasma mirrors for ultrahigh-intensity optics

C. THAURY[1], F. QUÉRÉ[1]*, J.-P. GEINDRE[2], A. LEVY[1], T. CECCOTTI[1], P. MONOT[1], M. BOUGEARD[1], F. RÉAU[1], P. D'OLIVEIRA[1], P. AUDEBERT[2], R. MARJORIBANKS[3] AND PH. MARTIN[1]

[1]Service des Photons, Atomes et Molécules, Commissariat à l'Energie Atomique, DSM/DRECAM, CEN Saclay, 91191 Gif-sur-Yvette, France
[2]Laboratoire pour l'Utilisation des Lasers Intenses, CNRS, Ecole Polytechnique, 91128 Palaiseau, France
[3]Department of Physics and Institute for Optical Sciences, University of Toronto, 60 St George Street, Toronto, Ontario M5S 1A7, Canada
*e-mail: fabien.quere@cea.fr

Published online: 15 April 2007; doi:10.1038/nphys595

Specular reflection is one of the most fundamental processes of optics. At moderate light intensities generated by conventional light sources this process is well understood. But at those capable of being produced by modern ultrahigh-intensity lasers, many new and potentially useful phenomena arise. When a pulse from such a laser hits an optically polished surface, it generates a dense plasma that itself acts as a mirror, known as a plasma mirror (PM). PMs do not just reflect the remainder of the incident beam, but can act as active optical elements. Using a set of three consecutive PMs in different regimes, we significantly improve the temporal contrast of femtosecond pulses, and demonstrate that high-order harmonics of the laser frequency can be generated through two distinct mechanisms. A better understanding of these processes should aid the development of laser-driven attosecond sources for use in fields from materials science to molecular biology.

Although plasmas are generally considered as unstable and hardly controllable media, during an ultrashort laser pulse—typically below 100 fs—this plasma only expands by a small fraction of the light wavelength, and thus behaves as a high-flatness mirror, leading to high-intensity specular reflection. Such a plasma mirror (PM) can be considered as one of the testbeds of high-intensity laser–plasma interaction physics, in particular because it avoids the complications associated with the nonlinear propagation of the intense laser light in a plasma.

Besides this fundamental interest, the potential of PMs as active high-intensity optical elements has long been recognized[1–3]. For instance, given the large change in reflectivity that occurs when an initially solid target is ionized and converted into a plasma, PMs can be used as laser-triggered ultrafast optical switches. This has been applied to shorten nanosecond pulses from CO_2 lasers down to the 100 fs range[1], to produce a time gate for the temporal characterization of ultrashort pulses[2], or, as we will illustrate in this paper, to improve the temporal contrast of ultrashort laser pulses[3–5].

In the past decade, research has been concentrated on the use of PMs in the relativistic interaction regime—that is, above a few 10^{18} W cm^{-2} at visible wavelengths, where the quivering motion of electrons in the laser field involves velocities of the order of the speed of light[6]. In this regime, PMs can be driven in a highly nonlinear regime, leading to the generation of very high-order harmonics of the incident light in the spectrum of the reflected beam, up to the extreme-ultraviolet and X-ray spectral ranges[7]. Theoretical studies predict that these harmonics are associated with intense trains of attosecond or even zeptosecond pulses[8,9], whereas isolated attosecond bursts are expected if intense few-cycle-long laser pulses are used[10–12]. This process seems to be the most promising alternative to high-order harmonic generation (HHG) in gases[13] to obtain attosecond pulses with higher pulse and photon energies[11]—a crucial step for the development of attosecond science. These theoretical predictions nevertheless remain to be validated experimentally.

However, applications as well as thorough experimental studies of PMs in the ultrahigh intensity regime have so far been hindered by the main weakness of ultraintense lasers, which is their temporal pedestal. When the main pulse intensity exceeds $10^{17}-10^{18}$ W cm^{-2}, the nanosecond light background surrounding this pulse, although typically $10^{6}-10^{8}$ times weaker, is intense enough to strongly ionize any solid target well before the main pulse. Because of the subsequent expansion of the resulting plasma, the main pulse, as short as it may be, ends up interacting with a long plasma density gradient, and no specular reflection is observed.

Here, we use a fully engineered double-plasma-mirror (DPM) set-up as an ultrafast high-dynamics optical switch to improve the temporal contrast by four orders of magnitude. The resulting high-contrast pulses are then used to reveal the basic mechanisms of HHG in the specular reflection of a PM driven at ultrahigh intensities, up to the relativistic regime. By using PMs in the role of both optical elements and objects of proper study, this paper demonstrates their dual fundamental and applied interest.

OPTICAL SWITCHING: FROM BASIC PHYSICS TO ENGINEERING

The temporal contrast of high-power lasers can be dramatically improved by using a surprisingly simple method, which consists of reflecting the laser beam on a dielectric target with an initially low reflectivity[3]. For an appropriate choice of beam focusing, the temporal pedestal is not intense enough to significantly affect this target, whereas the much more intense main laser pulse induces a strong ionization, through nonlinear excitation processes. A plasma is thus created within some femtoseconds at the rising edge of the main pulse. The target reflectivity strongly increases when this plasma becomes dense enough to screen the incident laser field, that is, when the electron density, n, exceeds the critical density, $n_c = m\varepsilon_0\omega_L^2/e^2$, characteristic of the laser frequency, ω_L, where e and m are the electron charge and mass and ε_0 is the vacuum dielectric constant. For an 800 nm laser wavelength and a sub-100 fs laser pulse, this typically requires intensities of a few 10^{14} W cm^{-2}.

In these conditions, the final result is a contrast enhancement ahead of the main pulse, with a magnitude that simply depends on the ratio of the plasma and initial target reflectivities.

To maximize the plasma reflectivity, the laser beam should be *s*-polarized—that is, with its electric field along the target's surface. The only source of absorption of laser energy by the plasma is then inverse Bremsstrahlung due to electron–ion collisions, and the final reflectivity, R_f, thus reaches about 70%. Using an antireflection-coated optical flat glass, with a typical reflectivity $R_i \approx 0.3\%$, a contrast improvement, R_f/R_i, of about two orders of magnitude is achieved[14].

Building on the comprehensive understanding of optical switching from PMs that has been achieved over the past few years[4,5,15], we have designed and permanently installed a DPM system at the output of the CEA-Saclay 10 TW, 60 fs Ti–Sa laser (see the Methods section and Supplementary Information, Fig. S1). The impact of this DPM is quantified in Fig. 1a: a high-dynamic-range ($\approx 10^{12}$) third-order autocorrelation[16] trace shows the temporal profile of the laser pulses obtained with and without this DPM. As expected, a contrast improvement of about four orders of magnitude is observed, producing pulse contrasts of 10^{10} for times up to $t = -10$ ps. This is one of the highest temporal contrasts achieved so far at a multi-TW power level[17].

The pedestal following the main pulse is also strongly decreased within a few picoseconds after the peak, owing to the hydrodynamics expansion of the plasma on the 10 ps timescale, which leads to its diffuse reflection by the PMs. However, this expansion is negligible on the 100 fs timescale, and hence the quality of the laser focal spot is not degraded by this DPM (see Supplementary Information, Fig. S2), which is an essential requirement for the applicability of this technique. As expected, the total reflectivity is measured to be about 50% for the main laser pulse.

This plasma-based technique can be easily implemented at the output of any laser chain, scaled to arbitrarily high laser powers, and cascaded in N stages, to gain $2N$ orders of magnitude in temporal contrast at a repetition rate of up to 1 Hz. It should thus become a crucial tool to routinely and practicably achieve the extreme temporal contrasts required for well-defined ultrahigh-intensity experiments on solid targets.

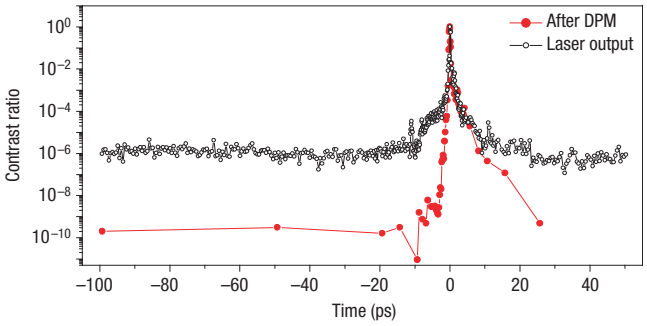

Figure 1 Temporal profile of the laser pulses delivered by a 10 TW, 60 fs laser system, in logarithmic scale, with and without the DPM. The signal at time 0 is set to 1 in both cases for an easier comparison between the two curves.

HHG FROM PLASMA MIRRORS

When PMs are driven in *s*-polarization and at moderate intensities, as in the previous application, the laser-driven dynamics is mostly along the target surface, and thus plasma electrons essentially behave as free electrons, simply quivering in the laser field. As the focused intensity is gradually increased up to the relativistic interaction regime, or when the laser field is *p*- rather than *s*-polarized, plasma electrons are driven across a steep electrostatic potential at the plasma–vacuum interface. This leads to a much richer and complex physics of the interaction, and to new effects, in particular the generation of high-order harmonics of the incident frequency in the spectrum of the reflected beam.

To illustrate this phenomenon, Fig. 2 shows the far-field spatial profile of the extreme-ultraviolet beam generated by a high-contrast *p*-polarized laser pulse focused at 5×10^{17} W cm^{-2} on an optically polished silica target (see the Methods section and Supplementary Information, Fig. S3). A collimated and smooth extreme-ultraviolet beam, which diverges about three times less than the fundamental beam, is clearly observed. This suggests a good phase-front quality, as well as a good transverse coherence of the harmonic source in the plane of the target surface, as opposed to what has been observed with picosecond laser pulses[18].

This result, as well as the DPM system presented above, demonstrates that plasmas can be used on ultrashort timescales as active optical components, keeping excellent optical quality even at ultrahigh laser intensities, and thus can be exploited to produce new light sources with remarkable properties—for example, shorter wavelengths and sub-femtosecond durations. From a fundamental perspective, this also leads to better-defined interaction conditions, hence considerably simplifying the physics and the interpretation of high-intensity experiments, as we now show by considering the basic physics of HHG on PMs.

For the past 30 years, many models have been proposed to explain HHG from plasmas[19–31], but clear experimental validations have so far remained scarce. Recent results tend to support two generation mechanisms, coherent wake emission[31,32] (CWE) and the relativistic oscillating mirror process[7,33], two processes which may in fact account for many former observations[14,34–37]. We now present new and strong experimental evidence for these two mechanisms, and show that they lead to harmonics with very

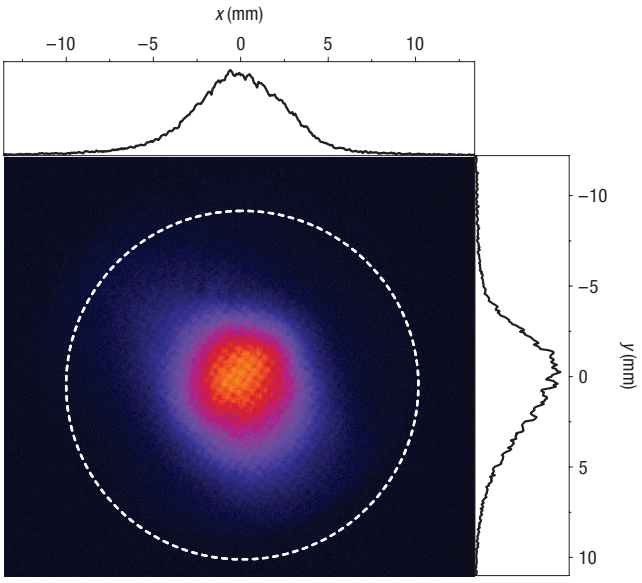

Figure 2 Spatial profile of the harmonic extreme-ultraviolet beam. This beam corresponds to the superposition of harmonics with orders $10 \leq p \leq 15$, 37 cm away from the target. The white dashed circle shows the spatial extension of the top-hat laser beam in the same plane. This extreme-ultraviolet beam has a divergence of 14 mrad (full-width at half-maximum).

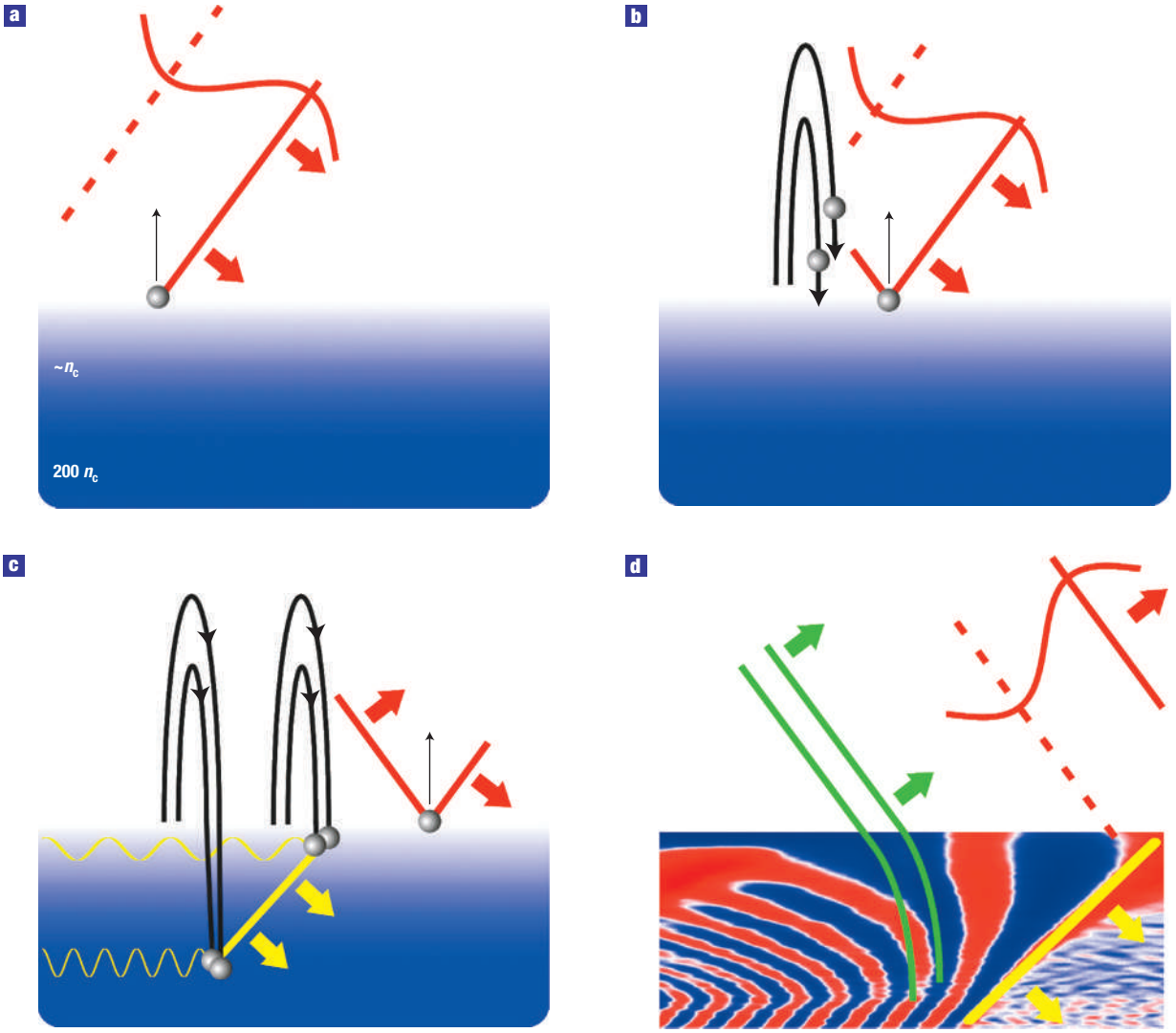

Figure 3 Schematic diagrams of different stages of the coherent wake emission process. a, Electrons around $n = n_c$ are pulled out of the plasma by the laser field. **b**, As the laser field decreases and changes sign, Brunel electrons are pushed back to the plasma. **c**, These electrons propagate in the overdense plasma, where they form an attosecond bunch. Owing to the oblique incidence of the laser beam, the superposition of the bunches formed at different times along the target surface results in an oblique density wavefront propagating into the plasma (thick yellow line). This density wave triggers plasma oscillations in its wake (yellow sinusoids). **d**, The wavefronts of these plasma oscillations, obtained from a PIC simulation. These plasma oscillations emit an attosecond light burst (wavefronts in green) as **k** becomes parallel to the surface.

different properties, thus enabling us to distinguish unambiguously between them.

COHERENT WAKE EMISSION

In p-polarization, the laser electric field has a large component, $E_\perp$, along the target normal. When it points inwards, some electrons near the surface are pulled out of the plasma (Fig. 3a). As soon as $E_\perp$ decreases, space–charge electrostatic fields drive some of these electrons back into the plasma (Fig. 3b,c), where they eventually no longer feel the laser field owing to plasma screening. These electrons thus propagate deeply into the plasma (Fig. 3c), and are responsible for a significant absorption of the laser pulse energy by steep density-gradient plasmas, an effect known as 'vacuum heating' or 'Brunel absorption'[38,39]. These Brunel electrons are also involved in harmonic generation through the recently proposed 'coherent wake emission' process[31], efficient down to intensities of a few 10^{15} W cm^{-2}.

Simple analytical models[38,39], as well as particles-in-cells (PIC) simulations[25] (see Supplementary Information and Movie S1), reveal that Brunel electrons that move further into vacuum come back to the plasma with larger velocities, and thus eventually overtake the electrons that had smaller excursions (Fig. 3b,c). By this trajectory crossing, they form an attosecond bunch that penetrates the plasma, with a new bunch once every optical cycle. These bunches of charge push the plasma background electrons, driving up electronic plasma oscillations throughout a range of densities in the steep gradient, $n(x)$, at the surface of the plasma (Fig. 3c).

An ensemble of linear plasma oscillations with space-dependent frequencies, $\omega_p(x) = \omega_L\sqrt{n/n_c}$, is thus coherently triggered. Owing to this spatial dependence, the wavevector **k** of this plasma wave has a time-varying direction (Fig. 3d). The wave, initially purely electrostatic and longitudinal ($\mathbf{E} \parallel \mathbf{k}$) when triggered by Brunel electrons, thus progressively acquires a partial transverse

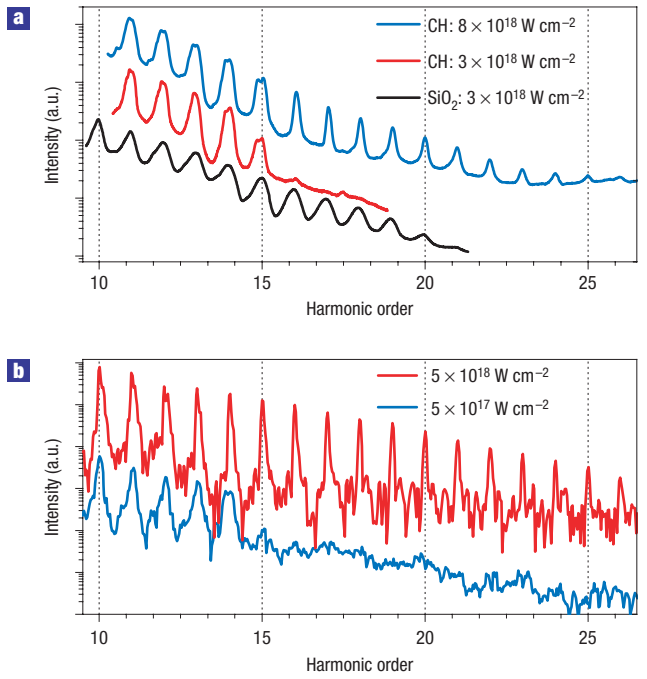

Figure 4 Harmonic spectra from plasma mirrors. a, Experimental spectra obtained by focusing high-intensity high-contrast 60 fs pulses on plastic and silica targets, for two laser intensities. The relative positions of the curves are arbitrary. **b**, Harmonic spectra from PIC simulations, for two different laser intensities, and a fixed plasma density $n_{max} = 220 \times n_c$.

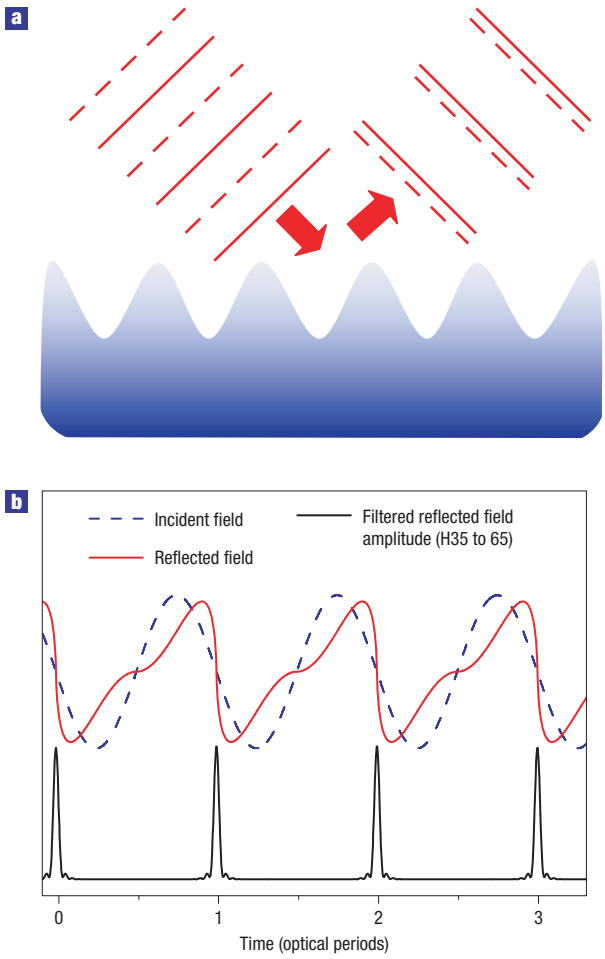

Figure 5 Relativistic oscillating mirror mechanism. a, Schematic diagram of the process. The solid and dashed lines show wavefronts of the incident and departing laser beam, corresponding respectively to minima and maxima of the electric field. **b**, Total electric field reflected by a ROM (red curve), and intensity envelope of the spectrally filtered radiation (from harmonics 35 to 65, black curve).

character, and can therefore radiate light[40]. Because this light emission is triggered once every optical cycle by returning Brunel electrons, the emitted spectrum consists of harmonics of the incident frequency. These harmonics extend as far as the maximum plasma frequency, ω_p^{max}, of the target, and hence up to the order $p_{CWE} = \sqrt{n_{max}/n_c}$, where n_{max} is the maximum plasma density. With typical values of n_{max} of a few hundred times n_c, this spectrum thus reaches into the extreme-ultraviolet regime.

This essential prediction of the CWE model is directly confirmed by Fig. 4a. The two lower curves show experimental harmonic spectra generated on silica and plastic targets at an intensity of about 3×10^{18} W cm^{-2}. In both cases, the maximum harmonic frequency corresponds to the expected maximum plasma frequency, ω_p^{max}, for fully ionized solid-density targets. A similar agreement has been obtained from aluminium and gold targets (see Supplementary Information, Fig. S4). This is crucial evidence for the CWE mechanism, which strongly reinforces the results presented in ref. 31.

For this mode conversion to be efficient, phase-matching between the plasma oscillations and the outgoing electromagnetic modes at the plasma vacuum interface is required. Such phase-matching can be shown to be fulfilled when $\mathbf{k}$ is parallel to the surface[31,41,42]. Because $\mathbf{k}$ is gradually rotating, this only occurs transiently, in a few-hundred-attosecond window following excitation by each electron burst (Fig. 3d): extreme-ultraviolet light is hence emitted in the form of a train of attosecond pulses. In analogy with the reflection of light pulses on 'chirped mirrors' used in conventional optics[43], each frequency, ω, originates from a different depth in the density gradient, where $\omega_p(x) = \omega$, and these attosecond pulses have a positive chirp progressively drifting to higher frequencies.

Harmonics produced by CWE now provide a direct way to investigate the dynamics of plasma mirrors driven at high intensity, and especially of Brunel electrons. Besides, PIC simulations predict that CWE has a typical conversion efficiency of 10^{-4} (ref. 31). Sources of extreme-ultraviolet and attosecond pulses in the 25–80 nm range with low divergence (down to a few milliradians), and energies in the 100 μJ range, could thus now be obtained by loosely focusing multi-TW laser pulses beyond a few 10^{15} W cm^{-2} on solid targets.

RELATIVISTIC OSCILLATING MIRROR

When the laser intensity is increased further, beyond a few 10^{18} W cm^{-2} at visible wavelengths, the laser-driven motion of the plasma surface becomes relativistic, leading to strong Doppler shifts of the laser light. As this oscillating surface chases the retreating optical phase fronts, it compresses the reflected electromagnetic field, distorting it from its original sinusoid (Fig. 5a,b). As this phase distortion repeats itself with the periodicity of the driving laser field, harmonics of the incident frequency then appear in the reflected beam. As shown in Fig. 5b, this harmonic comb is again associated with a train of attosecond pulses, each pulse

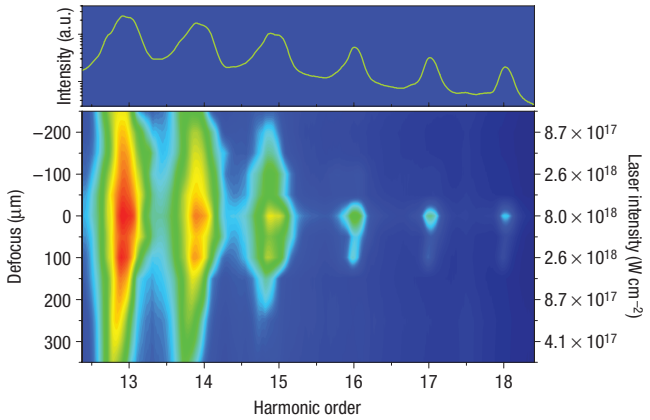

Figure 6 Harmonic spectrum dependency on the laser intensity. Harmonic spectra obtained on plastic plotted in logarithmic scale as a function of distance between the target surface and the laser best focus. The right axis shows the estimated peak intensity corresponding to each position. The intensity at the best focus is about 8×10^{18} W cm^{-2}, and the upper panel shows the spectrum obtained at this intensity. Each spectrum is averaged on 5 laser shots, and measurements were carried out for 10 focusing positions.

corresponding to an outward excursion of the plasma surface. This is the so-called 'relativistic oscillating mirror' (ROM) process, which was identified theoretically more than a decade ago[24,26]. As opposed to CWE, the maximum harmonic order that can be obtained by this process now strongly depends on the laser intensity[9,30] and can thus exceed the plasma frequency.

To get experimental evidence of this process, the high-contrast pulses obtained from the DPM were focused at the highest intensities currently achievable in our laboratory, using a parabolic mirror with an $f/4$ numerical aperture. The top-most curve in Fig. 4a shows the harmonic spectrum obtained from the same plastic target as before, now delivering intensities approaching 10^{19} W cm^{-2}, that is, well beyond the relativistic threshold. CWE harmonics are still observed up to the maximum plasma frequency $\omega_p^{max} = 15\omega_L$ of the target, but some harmonics now appear above ω_p^{max}. We attribute these harmonics to the ROM mechanism, and now present clear experimental observations that unambiguously support this interpretation.

SPECTRAL PROPERTIES OF CWE AND ROM HARMONICS

On the upper HHG spectrum of Fig. 4a, one striking feature is that ROM harmonics, that is, those with $p > 15$, are about half the spectral width of those generated by CWE on any material (see Supplementary Information, Fig. S5). This difference in spectral width is also observed in simulations. Figure 4b shows harmonic spectra obtained from PIC simulations, for two laser intensities, 5×10^{17} W cm^{-2} and 5×10^{18} W cm^{-2}, and a maximum plasma density, $n_{max} = 220 \times n_c$. At the lower intensity, broad CWE harmonics are observed up to order $p_{CWE} = \sqrt{n_{max}/n_c}$, as in the experiment. At the higher intensity, narrow harmonics appear for orders above p_{CWE}, which PIC simulations allow us to clearly attribute to the ROM process.

If the individual harmonics were all Fourier-transform limited, CWE harmonics would have to be generated during a shorter time period than ROM harmonics, to account for these differences in spectral width. This is inconsistent with the much stronger intensity dependence of this second mechanism, as we will see below. PIC simulations show that these differences in spectral width are rather due to the very different chirps of the individual harmonics generated by these two mechanisms. Considering CWE, in the non-relativistic regime, the peak velocity of Brunel electrons varies in time, according to the intensity envelope of the laser pulse. As a result, the delay between the formation of an electron bunch by returning Brunel electrons at $n \approx n_c$, and the generation of the associated attosecond pulse at $n \gg n_c$, is time dependent, and the period between successive attosecond pulses in the train generated by this process shifts gradually. CWE harmonics are hence not Fourier-transform limited, but negatively chirped[31,44], and this accounts for their large spectral width. In contrast, the chirp of the harmonics from ROM is much smaller, owing to the much better periodicity of the associated attosecond pulse train, imposed by the regular oscillations of the plasma surface, in turn tied in phase to the driving laser.

INTENSITY DEPENDENCES OF CWE AND ROM

The CWE and ROM mechanisms are also characterized by very different dependences on laser intensity. This is illustrated in Fig. 6, which shows the intensity dependence of the harmonic spectrum from a plastic target, measured by varying the distance between the target surface and the best focus of the laser beam (Fig. 6). CWE is a quasi-linear conversion process, the overall efficiency of which depends only weakly on laser intensity[31]. Thus, harmonics below order 15 vary very weakly with changing laser intensity, and are still clearly present below the relativistic threshold. On the contrary, harmonics beyond order 15 vanish sharply and almost simultaneously as soon at the target is moved away from the best focus by a distance of the order of the Rayleigh length—an intensity change of about 50%. They are only observed for intensities approaching 10^{19} W cm^{-2}. This is highly characteristic of the ROM mechanism, a relativistic process that is here driven near its intensity threshold, and is therefore highly nonlinear.

OUTLOOK

Despite more than 20 years of investigations on HHG from plasmas, so far clear signatures of the underlying mechanisms could generally not be teased out from the often uncontrollable—and sometimes unknowable—conditions of the plasma produced. This is now possible using ultrashort high-temporal-contrast ultraintense laser pulses. In addition, this interaction regime is of high interest for the development of extreme-ultraviolet sources from plasmas, as harmonics are then emitted as a collimated light beam. This is a first step towards a source of intense attosecond pulses, that is needed for the development of the new attosecond science[11]. In this respect, the ROM mechanism is particularly appealing, as it could be used to generate intense and extremely short attosecond pulses with photon energies up to the kiloelectron volt range[7].

In a more general context, many schemes have now been proposed, or even validated in experiments, to put plasmas to work as high-intensity optical elements, such as in the case of the plasma-based optical switches presented in this paper. Such 'plasma optics' are for instance predicted to further amplify ultraintense lasers[45], to tailor[46] or to temporally compress ultrashort pulses down to the few femtosecond range[47,48], and to generate ultrashort coherent radiation from the terahertz[41,42] to X-ray range. The present work shows that this interplay between plasmas as objects of fundamental study, and plasmas as high-intensity optical elements, is a very promising route to explore new frontiers of high-intensity laser–matter interaction.

METHODS

DOUBLE-PLASMA-MIRROR SET-UP

The DPM set-up is located in a vacuum chamber (see Supplementary Information, Fig. S1), inserted between the experimental chamber and the

compressor of a 10 TW, 60 fs, 10 Hz chirped-pulse-amplification Ti–Sa laser. The 700 mJ laser pulses are focused by an off-axis parabolic mirror of 1.25 m focal length, midway between two antireflection-coated plates, located a few centimetres apart (see Supplementary Information, Fig. S1). The laser beam is horizontally polarized, and is thus in *s*-polarization with respect to the plane of incidence on these two plates, which is vertical. This maximizes the reflectivity of these plasma mirrors once they are triggered[4,5]. The laser beam size on the plates is about 1 mm, leading to fluences of 90 and 70 J cm^{-2} on the first and second PM, respectively. The divergent beam reflected by these two PMs is collimated by a second off-axis parabola, and is then directed to the experimental chamber, where it can be used for high-contrast, high-intensity experiments. Owing to the ablation of the antireflection coating induced by the main laser pulse, the dielectric plates are translated by a few millimetres after each shot. However, this device can operate continuously at a repetition rate of up to 1 Hz for about 2,000 shots, before the antireflection plates have to be changed. This DPM can easily be bypassed owing to two retractable mirrors (see Supplementary Information, Fig. S1), thus making it possible to investigate the influence of the temporal contrast in high-intensity experiments. Supplementary Information, Fig. S2 shows the focal spot of the 10 TW laser beam (measured at full power), with and without the DPM. These two images clearly demonstrate that the spatial quality of the beam is not degraded by the DPM.

MEASUREMENTS OF THE EXTREME-ULTRAVIOLET BEAM FAR-FIELD SPATIAL PROFILE

High-order harmonics are first generated by reflection on a solid target at high intensity (see Supplementary Information, Fig. S3). The resulting beam then reflects at grazing incidence ($\theta_i = 80°$) on two dielectric plates with a broadband antireflection coating around $\lambda = 800$ nm, the fundamental wavelength of the initial laser pulse. At this wavelength, the total reflectivity of the two plates is less than 10^{-4}, whereas it is about 50% for harmonics 10–20, owing to the grazing incidence[49]. The remaining fundamental frequency and low-order harmonics ($p \leq 9$) are then eliminated using a 200-nm-thick tin filter. This filter transmits light only for frequencies between the 10th and 15th harmonics of the laser beam, with a maximum transmission of about 20% around order 14. The spatial profile of the resulting extreme-ultraviolet beam is measured using microchannel plates, coupled to a phosphor screen that is imaged on a CCD (charge-coupled device) camera. This microchannel plate detector is sensitive only to wavelengths smaller than 110 nm (≈7th harmonic), which definitely excludes any contribution of the fundamental or low-order harmonics to the measured signal.

PIC SIMULATIONS

The results presented in Fig. 4b have been obtained using the $1\frac{1}{2}$-D relativistic PIC code EUTERPE[50], which allows for oblique incidence of the laser beam by a transformation to a moving frame. Both electrons and ions are mobile, and all results are converted back into the laboratory frame at the end of the simulations. Because these simulations neglect several spatial effects (laser intensity distribution in the focal spot, diffraction of the harmonic beam from the target to the spectrometer), they cannot be expected to exactly reproduce measured spectra such as the upper curve of Fig. 4a. This can explain why, in the simulation corresponding to the highest intensity (Fig. 4b), harmonics below p_{CWE} are narrower than what is observed experimentally.

Received 20 November 2006; accepted 16 March 2007; published 15 April 2007.

References

1. Rolland, C. & Corkum, P. B. Generation of 130-fsec midinfrared pulses. *J. Opt. Soc. Am. B* **3**, 1625–1629 (1986).
2. Teubner, U., Wagner, U. & Forster, E. Sub-10 fs gating of optical pulses. *J. Phys. B* **34**, 2993–3002 (2001).
3. Kapteyn, H. C., Murnane, M. M., Szoke, A. & Falcone, R. W. Prepulse energy suppression for high-energy ultrashort pulses using self-induced plasma shuttering. *Opt. Lett.* **16**, 490–492 (1991).
4. Doumy, G. *et al.* Complete characterization of a plasma mirror for the production of high-contrast ultraintense laser pulses. *Phys. Rev. E* **69**, 026402 (2004).
5. Dromey, B., Kar, S., Zepf, M. & Foster, P. The plasma mirror—A subpicosecond optical switch for ultrahigh power lasers. *Rev. Sci. Instrum.* **75**, 645–649 (2004).
6. Mourou, G. A., Tajima, T. & Bulanov, S. V. Optics in the relativistic regime. *Rev. Mod. Phys.* **78**, 309–371 (2006).
7. Dromey, B. *et al.* High harmonic generation in the relativistic limit. *Nature Phys.* **2**, 456–459 (2006).
8. Plaja, L., Roso, L., Rzazewski, K. & Lewenstein, M. Generation of attosecond pulse trains during the reflection of a very intense laser on a solid surface. *J. Opt. Soc. Am. B* **15**, 1904–1911 (1998).
9. Gordienko, S., Pukhov, A., Shorokhov, O. & Baeva, T. Relativistic doppler effect: Universal spectra and zeptosecond pulses. *Phys. Rev. Lett.* **93**, 115002 (2004).
10. Naumova, N. M., Nees, J. A., Sokolov, I. V., Hou, B. & Mourou, G. A. Relativistic generation of isolated attosecond pulses in a λ^3 focal volume. *Phys. Rev. Lett.* **92**, 063902 (2004).
11. Tsakiris, G., Eidmann, K., Meyer-ter-Vehn, J. & Krausz, F. Route to intense single attosecond pulses. *New J. Phys.* **8**, 19 (2006).
12. Baeva, T., Gordienko, S. & Pukhov, A. Relativistic plasma control for single attosecond x-ray burst generation. *Phys. Rev. E* **74**, 065401 (2006).
13. Agostini, P. & DiMauro, L. The physics of attosecond light pulses. *Rep. Prog. Phys.* **67**, 813 (2004).
14. Monot, P. *et al.* High-order harmonic generation by nonlinear reflection of an intense high-contrast laser pulse on a plasma. *Opt. Lett.* **29**, 893–895 (2004).
15. Watts, I. *et al.* Measurements of relativistic self-phase-modulation in plasma. *Phys. Rev. E* **66**, 036409 (2002).
16. Luan, S., Hutchinson, M., Smith, R. & Zhou, F. High dynamic-range 3rd-order correlation-measurement of picosecond laser-pulse shapes. *Meas. Sci. Technol.* **4**, 1426–1429 (1993).
17. Chvykov, V., Rousseau, P., Reed, S., Kalinchenko, G. & Yanovsky, V. Generation of 10^{11} contrast 50 TW laser pulses. *Opt. Lett.* **31**, 1456–1458 (2006).
18. Zhang, J. *et al.* Coherence and bandwidth measurements of harmonics generated from solid surfaces irradiated by intense picosecond laser pulses. *Phys. Rev. A* **54**, 1597–1603 (1996).
19. Carman, R. L., Forslund, D. W. & Kindel, J. M. Visible harmonic emission as a way of measuring profile steepening. *Phys. Rev. Lett.* **46**, 29–32 (1981).
20. Carman, R. L., Rhodes, C. K. & Benjamin, R. F. Observation of harmonics in the visible and ultraviolet created in CO_2-laser-produced plasmas. *Phys. Rev. A* **24**, 2649–2663 (1981).
21. Bezzerides, B., Jones, R. D. & Forslund, D. W. Plasma mechanism for ultraviolet harmonic radiation due to intense CO_2 light. *Phys. Rev. Lett.* **49**, 202–205 (1982).
22. Grebogi, C., Tripathi, V. K. & Chen, H. Harmonic generation of radiation in a steep density profile. *Phys. Fluids* **26**, 1904–1908 (1983).
23. Wilks, S. C., Kruer, W. L. & Mori, W. B. Odd harmonic-generation of ultra-intense laser-pulses reflected from an overdense plasma. *IEEE Trans. Plasma Sci.* **21**, 120–124 (1993).
24. Bulanov, S. V., Naumova, N. M. & Pegoraro, F. Interaction of an ultrashort, relativistically strong laser-pulse with an overdense plasma. *Phys. Plasmas* **1**, 745–757 (1994).
25. Gibbon, P. Harmonic generation by femtosecond laser-solid interaction: A coherent water-window light source? *Phys. Rev. Lett.* **76**, 50–53 (1996).
26. Lichters, R., Meyer-ter-Vehn, J. & Pukhov, A. Short-pulse laser harmonics from oscillating plasma surfaces driven at relativistic intensity. *Phys. Plasmas* **3**, 3425–3437 (1996).
27. von der Linde, D. & Rzàzewski, K. High-order optical harmonic generation from solid surfaces. *Appl. Phys. B* **63**, 499–506 (1996).
28. Ondarza-Rovira, R. & Boyd, T. J. M. Plasma harmonic emission from laser interactions with dense plasma. *Phys. Plasmas* **7**, 1520–1530 (2000).
29. Pirozhkov, A. S. *et al.* Attosecond pulse generation in the relativistic regime of the laser-foil interaction: The sliding mirror model. *Phys. Plasmas* **13**, 013107 (2006).
30. Baeva, T., Gordienko, S. & Pukhov, A. Theory of high-order harmonic generation in relativistic laser interaction with overdense plasma. *Phys. Rev. E* **74**, 046404 (2006).
31. Quéré, F. *et al.* Coherent wake emission of high-order harmonics from overdense plasmas. *Phys. Rev. Lett.* **96**, 125004 (2006).
32. Teubner, U. *et al.* Harmonic emission from the rear side of thin overdense foils irradiated with intense ultrashort laser pulses. *Phys. Rev. Lett.* **92**, 185001 (2004).
33. Watts, I. *et al.* Dynamics of the critical surface in high-intensity laser-solid interactions: Modulation of the XUV harmonic spectra. *Phys. Rev. Lett.* **88**, 155001 (2002).
34. von der Linde, D. *et al.* Generation of high-order harmonics from solid surfaces by intense femtosecond laser pulses. *Phys. Rev. A* **52**, R25 (1995).
35. Norreys, P. A. *et al.* Efficient extreme UV harmonics generated from picosecond laser pulse interactions with solid targets. *Phys. Rev. Lett.* **76**, 1832–1835 (1996).
36. Tarasevitch, A. *et al.* Generation of high-order spatially coherent harmonics from solid targets by femtosecond laser pulses. *Phys. Rev. A* **62**, 023816 (2000).
37. Teubner, U. *et al.* Anomalies in high-order harmonic generation at relativistic intensities. *Phys. Rev. A* **67**, 013816 (2003).
38. Brunel, F. Not-so-resonant, resonant absorption. *Phys. Rev. Lett.* **59**, 52–55 (1987).
39. Bonnaud, G., Gibbon, P., Kindel, J. & Williams, E. Laser interaction with a sharp-edged overdense plasma. *Laser Part. Beams* **9**, 339–354 (1991).
40. Jackson, J. *Classical Electrodynamics* (Wiley, New York, 1998).
41. Sheng, Z. M., Mima, K., Zhang, J. & Sanuki, H. Emission of electromagnetic pulses from laser wakefields through linear mode conversion. *Phys. Rev. Lett.* **94**, 095003 (2005).
42. Sheng, Z. M., Mima, K. & Zhang, J. Powerful terahertz emission from laser wake fields excited in inhomogeneous plasmas. *Phys. Plasmas* **12**, 123103 (2005).
43. Szipocs, R., Ferencz, K., Spielmann, C. & Krausz, F. Chirped multilayer coatings for broad-band dispersion control in femtosecond lasers. *Opt. Lett.* **19**, 201–203 (1994).
44. Varju, K. *et al.* Frequency chirp of harmonic and attosecond pulses. *J. Mod. Opt.* **52**, 379–394 (2005).
45. Fisch, N. J. & Malkin, V. M. Generation of ultrahigh intensity laser pulses. *Phys. Plasmas* **10**, 2056–2063 (2003).
46. Wu, H. C., Sheng, Z. M., Zhang, Q. J., Cang, Y. & Zhang, J. Manipulating ultrashort intense laser pulses by plasma Bragg gratings. *Phys. Plasmas* **12**, 113103 (2005).
47. Faure, J. *et al.* Observation of laser-pulse shortening in nonlinear plasma waves. *Phys. Rev. Lett.* **95**, 205003 (2005).
48. Stibenz, G., Zhavoronkov, N. & Steinmeyer, G. Self-compression of millijoule pulses to 7.8 fs duration in a white-light filament. *Opt. Lett.* **31**, 274–276 (2006).
49. Takahashi, E. J., Hasegawa, H., Nabekawa, Y. & Midorikawa, K. High-throughput, high-damage-threshold broadband beam splitter for high-order harmonics in the extreme-ultraviolet region. *Opt. Lett.* **29**, 507–509 (2004).
50. Bonnaud, G. & Reisse, G. Particle code study of the influence of non-monochromaticity of laser-light on stimulated Raman-scattering in laser-irradiated plasmas. *Nucl. Fusion* **26**, 633–646 (1986).

Acknowledgements

Financial support from the Conseil Général de l'Essonne (ASTRE program) is acknowledged. Correspondence and requests for materials should be addressed to F.Q. Supplementary Information accompanies this paper on www.nature.com/naturephysics.

Competing financial interests

The authors declare no competing financial interests.